

# Validity of the Additive White Gaussian Noise Model for Quasi-Linear Long-Haul Return-to-Zero Optical Fiber Communications Systems

John Zweck and Curtis R. Menyuk, *Fellow, IEEE*

**Abstract**—In this paper, we study the validity and limitations of the additive white Gaussian noise (AWGN) model in quasi-linear, long-haul, return-to-zero, direct-detection optical fiber communications systems. Our approach is to compare bit-error ratios (BERs) computed using the additive white Gaussian noise method to those obtained using standard and multicanonical Monte Carlo (MMC) simulations and to a noise-linearization method, referred to as the noise covariance matrix (NCM) method. We show that the AWGN method provides a very good approximation to the actual system BER for power levels and dispersion profiles that are used in typical modern-day quasi-linear systems. For example, the BER obtained using the AWGN method is within a factor of 4 of the actual system BER computed using MMC simulations for a realistic 10 Gb/s, 6000 km system based on dispersion-shifted fiber in which the peak signal power at the transmitter is 1 mW and the absolute residual dispersion at the receiver is less than 200 ps/nm. However, when the peak power is increased to about 4 mW, or the average map dispersion is zero and the absolute residual dispersion exceeds 200 ps/nm, the AWGN and NCM methods may simultaneously breakdown due to a combination of nonlinear signal-noise and noise-noise interactions during transmission. In addition, for a 5000 km system based on low-nonlinearity  $D_+$  and  $D_-$  fiber with an average map dispersion that is 4% of the dispersion variation within the map, and that operates at a peak power of 5 mW, we find that the BERs obtained using the AWGN and NCM methods are about 500 times smaller than the actual system BER computed using MMC simulations.

**Index Terms**—Amplifier noise, Monte Carlo methods, optical fiber communication, optical Kerr effect.

## I. INTRODUCTION

THE purpose of this paper is to study the validity of the additive white Gaussian noise (AWGN) model in quasi-linear, long-haul, return-to-zero (RZ), direct-detection optical fiber communications systems. With the AWGN model [1], the noise-free signal is propagated through the optical fibers independently of the noise and combined with AWGN in the square-law photodetector at the receiver. Consequently, the model ignores any nonlinear interactions involving the noise

during fiber propagation. In particular, it ignores any parametric gain of the noise due to its nonlinear interaction with the signal. Although the AWGN model is widely used in the design and performance evaluation of optical fiber communications systems, there is no literature reporting on a comprehensive validation of the model.

Parametric gain has been widely studied in the context of optical fiber communications, both experimentally and using modeling, analysis, and simulation. Parametric gain is a four-wave mixing process in optical fiber in which energy is transferred from the signal to the amplified spontaneous emission (ASE) noise that is produced by optical amplifiers [2]. This process results in broadening and coloring of the power spectrum of the optical noise and is most efficient when the chromatic dispersion is close to zero. Chromatic dispersion converts the phase noise generated by the parametric gain process into amplitude noise. In direct-detection systems, this amplitude noise causes fluctuations in the received electrical current that can be statistically different from those due to additive white Gaussian noise. Consequently, parametric gain can potentially result in a different bit-error ratio (BER) than would be predicted by the AWGN model.

Hui *et al.* [3], [4] developed a model for parametric gain in which they assumed a continuous-wave (CW) signal. By linearizing the propagation of the noise about the analytically known evolution of the CW signal, they were able to calculate the optical power spectrum of the noise as well as the relative intensity noise spectrum after the square-law photodetector. At each frequency, the relative intensity noise quantifies the amount by which parametric gain changes the noise power after the photodetector relative to that predicted by the AWGN model. Hui *et al.* used their model to show that the amount of postdispersion compensation has a significant effect on the relative intensity noise spectrum. This model has been experimentally verified [4]–[6] and widely adapted and used.

In similar approaches to that of Hui, Carena *et al.* [7] and Bosco *et al.* [8], [9] separated the noise in each frequency into a component that is inphase with the CW signal together with a quadrature component. Due to the parametric gain process, the inphase and quadrature components of the noise grow at different rates during propagation and cross correlations can be introduced between the two components. In a direct-detection receiver, the signal beats only with the inphase component of the noise and is independent of the quadrature component. Depending on the details of the dispersion profile, it is possible to decrease the inphase noise component relative to the quadrature

Manuscript received July 18, 2008; revised November 18, 2008. First published April 17, 2009; current version published July 24, 2009. This work was supported by the National Science Foundation under Grant ECS-0400535.

J. Zweck is with the Department of Mathematics and Statistics, University of Maryland Baltimore County, Baltimore, MD 21250 USA (e-mail: zweck@umbc.edu).

C. R. Menyuk is with the Department of Computer Science and Electrical Engineering, University of Maryland Baltimore County, Baltimore, MD 21250 USA (e-mail: menyuk@umbc.edu).

Digital Object Identifier 10.1109/JLT.2008.2010514

component, which can result in a decrease in the BER relative to that predicted by the AWGN model. This phenomenon, which is called noise squeezing, has been observed experimentally [10].

Holzlohner *et al.* [11]–[13] generalized these CW-linearization methods to the case of an arbitrary, data-modulated signal. Since the method involves the propagation of the covariance matrix of the ASE noise through the transmission system using a linearization about the signal, we will refer to it as the noise covariance matrix (NCM) method. The NCM method was successfully applied to a single-channel, highly nonlinear dispersion-managed soliton system for which the AWGN model is not valid. It has also been adapted and applied to model quasi-linear wavelength-division multiplexed (WDM) RZ systems [13], [14].

Serena *et al.* [15], [16] showed that the linearization methods discussed earlier can breakdown when the average signal power is larger than about 5 dBm, and the optical signal-to-noise ratio (OSNR) is smaller than about 15 dB in long-haul systems that are more than several hundred kilometers in length. In these situations, the inphase noise power spectral density is larger near the central frequency of the channel than is predicted by the linearization models. In the case of a CW signal, Serena *et al.* corrected for this deficiency by adding quadratic terms in the noise into the linearized frequency-domain noise propagation equation. By deriving an analytical formula in the case that the residual dispersion is zero, they showed that the inphase ASE noise power spectral density at the central frequency of the channel is inversely proportional to the OSNR and is directly proportional to the fourth power of the average received nonlinear phase [16]. Therefore, it grows rapidly once the signal power exceeds a threshold value that they derive. They demonstrated that the noise inflation near the central frequency has a significant effect on long-haul nonreturn-to-zero (NRZ) systems employing forward error correction. Recently, Secondini *et al.* [17] developed a promising combined regular-logarithmic perturbation method that also retains quadratic noise terms but as in Serena's work assumes a CW signal.

Although a great deal of effort has gone into modeling and clarifying the physical consequences of the parametric gain, little work has been reported that studies the degree to which parametric gain actually affects the BER in realistic communications systems. A notable exception is the work of Serena *et al.* on NRZ systems [16]. Put another way, it is important to understand when the widely used AWGN model is valid and to explore its limitations. In this paper, we report on a systematic study to determine the accuracy with which the AWGN model computes the BER for realistic quasi-linear, long-haul, RZ, direct-detection systems. Our approach is to compare the results obtained using the AWGN method to those obtained using standard Monte Carlo (StdMC) and multicanonical Monte Carlo (MMC) simulations [18]–[21] and with the NCM method. The AWGN and NCM methods incorporate a receiver model that accurately computes the probability density functions (pdfs) of the received current in each bit using Karhunen–Loève expansions as in [11], [22], [23]. MMC simulations are crucial to our study as they enable the BER to be accurately computed using a realistic system model.

Briefly, our conclusion is that the AWGN method provides a very good approximation to the actual system BER for power levels and dispersion profiles that are used in typical modern-day quasi-linear systems. Specifically, we show that the BERs obtained using the AWGN and NCM methods are within a factor of 4 of the actual system BER computed using MMC simulations for a realistic 10 Gb/s, 6000 km system based on dispersion-shifted fiber (DSF) in which the peak signal power at the transmitter is 1 mW and the absolute residual dispersion at the receiver is less than 200 ps/nm. However, when the peak power is increased to about 4 mW, or the average map dispersion is zero and the absolute residual dispersion exceeds 200 ps/nm, the AWGN and NCM methods may simultaneously breakdown due to the combination of nonlinear signal–noise and noise–noise interactions. In addition, for a 5000 km system based on low-nonlinearity  $D_+$  and  $D_-$  fiber with an average map dispersion that is 4% of the dispersion variation within the map, and which operates at a peak power of 5 mW, we find that the BERs obtained using the AWGN and NCM methods are about 500 times smaller than the actual system BER computed using MMC simulations. We ascribe the breakdown in the AWGN and NCM methods to the noise inflation process described by Serena *et al.* and observe that when the peak power is about 4 mW, the noise inflation can affect the system performance even when the average dispersion is far from zero.

## II. NOISE MODELS

In this section, we review the four methods—two deterministic and two stochastic—that we used to calculate the BER due to the interaction between signal and noise during transmission and in the receiver. The deterministic methods that we used are the AWGN and the NCM methods. Although they do not suffer from stochastic uncertainty, these two methods do not include all possible interactions between signal and noise during transmission. On the other hand, the two stochastic methods, namely, the MMC and StdMC methods, can model all possible interactions involving the signal and the noise but typically at the cost of a significant increase in computational time.

In all the four methods, we modeled the propagation of light through optical fibers using the scalar generalized nonlinear Schrödinger (NLS) equation including fiber loss, chromatic and third-order dispersion, and the Kerr nonlinearity. We numerically solved the NLS equation using the Fourier split-step method and adaptively controlled the step sizes using either the third-order local error or walk-off criterion [24].

We made several simplifications, none of which should affect our conclusions. First, we modeled the optical amplifiers using a simple fixed-gain model, rather than using a more realistic gain-saturated amplifier model. In addition, we assumed that the amplifier gain is flat across the simulated bandwidth of the channel. Second, we did not include polarization effects and we chose the noise to be scalar rather than vector-valued, that is we assumed that the signal and noise are both polarized and that their polarization states are the same. As a consequence our model does not include the noise that is added orthogonal to the signal in Jones space and does not account for any depolarization of the signal due to polarization-mode dispersion. Although the system performance computed using any of the

four noise models is somewhat better under this assumption than without it, the relative difference between the BERs computed using the AWGN method and any of the other three methods is greater under our assumption than without it because nonlinear interactions between orthogonal polarization states are weaker than those within a given polarization state [2], [25]. Consequently, this assumption does not affect our overall conclusion that the AWGN model is valid in typical modern-day quasi-linear systems. Finally, rather than modeling all or several channels of a WDM system, we restricted our attention to modeling a single channel of a WDM system. We limited ourselves to single-channel simulations since MMC simulations of WDM systems are very time consuming and because inter-channel nonlinear signal–noise interactions are much less significant than intrachannel interactions. Moreover, nonlinear interchannel signal–signal interactions usually become important at lower powers than nonlinear intrachannel signal–noise interactions [26]. Single-channel simulations allowed us to focus on signal–noise and noise–noise interactions.

#### A. Deterministic Models

In both the AWGN and NCM methods, we express the signal as the sum of a noise-free signal and noise. In both methods, we ignore any nonlinear effect that the noise has on the noise-free signal in the optical fiber and propagate the noise-free signal through the fibers by numerically solving the NLS equation.

In the AWGN method ([1], 8.6.4), we model the noise-free signal using a full time-domain representation,  $u$ . We ignore all nonlinear effects that the noise-free signal has on the noise. Therefore, since we are also ignoring all polarization effects and we are assuming that the amplifier gain is flat, we can characterize the noise by the noise spectral density,  $N_{\text{ASE}}$ . The noise-free signal is initialized at the transmitter using the binary data sequence and the optical pulse shape, and the noise spectral density is initially set to  $N_{\text{ASE}} = 0$ . If, as is done here, we ignore gain saturation effects in the optical amplifiers, the noise-free signal and the noise spectral density can be independently propagated through the transmission system. The noise-free signal is propagated through each fiber span by numerically solving the NLS equation, and at each optical amplifier,  $u^{\text{out}} = \sqrt{G}u^{\text{in}}$ , where  $G$  is the linear power gain. Within each fiber span, the noise undergoes loss so that  $N_{\text{ASE}}^{\text{out}} = LN_{\text{ASE}}^{\text{in}}$ , where  $L$  is the total linear power loss in the span. In each amplifier,  $N_{\text{ASE}}^{\text{out}} = GN_{\text{ASE}}^{\text{in}} + (G-1)n_{\text{sp}}h\omega$ , where  $n_{\text{sp}}$  is the spontaneous emission factor,  $h$  is Planck's constant, and  $\omega$  is the central frequency of the noise-free signal. At the receiver, the noise-free signal and the noise spectral density are combined to compute the BER using the receiver model described later. Although we have not done so here, the AWGN model can be extended to include nonflat gain and gain saturation in the optical amplifiers, as well as polarization effects [27], [28].

With the NCM method [11]–[13], we include the effect that the signal has on the noise due to the Kerr nonlinearity in the fiber. However, we assume that during transmission the nonlinear interaction of the noise with itself is negligible. Under this assumption, the propagation of the noise can be linearized about that of the noise-free signal, i.e., the propagation of the noise is

governed by a linear partial differential equation in which the coefficients depend on the noise-free signal. As a consequence, the noise remains multivariate-Gaussian-distributed as it propagates. Therefore, since the mean of the optical noise is zero, the noise is characterized by its covariance matrix. Holzlöhner *et al.* [13] developed a deterministic perturbative method to propagate the covariance matrix through the transmission system, which we use in our simulations.

Holzlöhner *et al.* [11] used Monte Carlo simulations to show that, for a highly nonlinear dispersion-managed soliton system, after a few thousand kilometers propagation, the noise is no longer multivariate-Gaussian distributed since the components of the noise that cause phase and timing jitter in the signal grow much more rapidly than other noise components. To overcome this limitation, the phase and timing jitter were periodically removed from the covariance matrix during propagation and treated separately [11]. Because direct-detection receivers are phase independent, the phase jitter was discarded. However, in [11], the timing jitter was reintroduced in the receiver. In our simulations, we investigated the effect of removing phase jitter in each bit using the method described in [13]. However, as in [13], we did not find it necessary to separate out timing jitter.

The covariance matrix of the noise is the real-valued  $2N \times 2N$  matrix  $\mathcal{K} = \langle \mathbf{a}\mathbf{a}^T \rangle$ , where  $\mathbf{a}$  is the real column vector consisting of the real and imaginary parts of the  $N$  lowest frequency components of the noise, and  $\mathbf{a}^T$  is its transpose. The number,  $N$ , of Fourier coefficients of the noise that must be included in  $\mathcal{K}$  is usually considerably less than the number of points,  $N_{\text{FFT}}$ , used to discretize the signal. However, to avoid incorrect results, it is necessary to choose  $N$  so that at the receiver on a log scale the power spectrum of the signal lies well below the average power spectrum of the noise,  $\mathcal{K}_{k,k} + \mathcal{K}_{k+N,k+N}$ , for the larger frequencies included in the covariance matrix. In our simulations, we used  $N_{\text{FFT}} = 1024$  and  $N = 300$ . This value of  $N$  was appropriate for the 35 GHz optical filter we used in the receiver. However, wider optical filters require larger values of  $N$ .

In the AWGN method, the NCM has the special form  $\mathcal{K} = (1/2)N_{\text{ASE}}\Delta\omega\mathcal{I}$ , where  $\Delta\omega$  is the frequency discretization and  $\mathcal{I}$  is the identity matrix.

We use the same *accurate receiver model* for both the AWGN and NCM methods. Our model is based on those in [11], [22], [23]. With this model, the pdfs of the received electrical current at the clock recovery time in each bit are computed from the noise-free signal, the NCM, and the transfer functions of the optical and electrical filters in the receiver. The pdf in each bit is a quadratic form of Gaussian vectors [11]. Such distributions have been extensively studied in the statistics literature [29]. In the special case of an integrate-and-dump receiver, the Gaussian distributions all have the same variance and so the pdfs are noncentral  $\chi^2$  distributions [30]. Analytical formulae for the asymptotic behavior of the tails of a quadratic form of Gaussian vectors are derived in [31], which could prove useful for obtaining analytical estimates of the BER. Here, though, we first use the method described in [11] to compute the characteristic function of the pdf in each bit. Then, we use the method of steepest descents to compute the pdf from its characteristic function using an approach similar to that in [22]. Next, we compute the average pdfs of the marks (i.e., ONEs) and spaces (i.e.,

ZEROs) and from those the minimum BER and optimal decision threshold. Finally, we calculate a  $Q$ -factor from the BER via the relation  $\text{BER} = (1/2)\text{erfc}(Q/\sqrt{2})$ , where  $\text{erfc}$  is the complement of the error function.

### B. Monte Carlo Methods

Since StdMC simulations are far too computationally expensive to calculate the low-probability tails of the voltage pdfs, we simply used them to estimate the mean and standard deviation of the voltage pdf in each bit. For this computation, we found that it was sufficient to use 800 samples per bit. We then approximated the pdfs of the electrically filtered current in each bit using a Gaussian distribution from which we calculated the average pdfs of the marks and spaces and the BER and  $Q$ -factor as above. We verified that when white Gaussian noise is added to a RZ signal without pattern dependence, the BER computed from the Gaussian pdfs is about 1.5 times larger than that computed using an accurate receiver model provided that the BER is smaller than about  $10^{-4}$  (also see [32]). However, the decision threshold is significantly smaller with the Gaussian pdfs.

To make more efficient use of Monte Carlo simulations, the MMC method increases the number of events in the low-probability tails of the pdf to be sampled by biasing the probability of their occurrence [18]–[20]. In our case, we sampled from the tails of the voltage pdf in a given bit by biasing the pdf of all ASE noise inputs at all amplifiers and all frequencies [21]. Note that here we include all frequencies in the signal—not just the ones that we included in the NCM. The MMC method is an iterative procedure that uses a choice of control quantity to update the biasing pdf for the next iteration. Within each iteration, the Metropolis algorithm is used to estimate the histogram of the pdf to be computed by drawing samples from the biasing pdf and weighting the probability of their occurrence by a likelihood ratio. The update procedure at the end of each iteration is designed so that as the number of iterations increases there tends to be an approximately equal number of hits in each bin of the histogram of the control quantity. If the control quantity is chosen to be well-correlated with the random variable whose pdf is being computed, then this design criterion will ensure that the pdf is well-sampled across its entire range, and in particular in the low-probability tails.

In [21], the authors chose to simultaneously sample all the pdfs of the spaces (marks) using the control quantity given by the maximum (minimum) of the received voltage in all the spaces (marks). Because of the possibility of large bit-pattern dependence in the noise-free signal, as in [14] we found it necessary to sample the pdf of a single bit using the control quantity given by the voltage in that bit. Because it is too computationally expensive to perform 32 MMC simulations to separately compute the pdf in each of the 32 bits, for all but one example, we restricted our MMC simulations to the computation of the pdfs of the *worst space* and *worst mark*, by which we mean the space (mark) with the highest (lowest) voltage at the clock time in the electrically filtered noise-free signal. For the exceptional example we computed the pdfs of the mark and space with the worst standard deviations, which we determined using a StdMC simulation.

Details of the implementation of the algorithm that we used can be found in [21]. In particular, we ran each MMC simulation until the following two stopping criteria were met. First, we required that the minimum value of the pdf was below a threshold value. This value was chosen to be about one order of magnitude less than the probability value at which the pdfs of the worst mark and worst space crossed in the AWGN simulation. Second, we required that the maximum relative error

$$\epsilon = \max_k \frac{|P_k^j - P_k^{j+1}|}{P_k^{j+1}} \quad (1)$$

was less than 10%. Here,  $P_k^j$  is the probability that the received current is in the  $k$ th bin of the histogram in iteration  $j$  of the MMC simulation. In our simulations, we required an average of 20 iterations to meet these stopping criteria for an average total number of  $1.5 \times 10^5$  samples for each space and  $7 \times 10^5$  samples for each mark.

In StdMC simulations, there is no correlation between the errors in the values in the different bins of the histogram. Consequently, the histogram fails to be smooth when it is statistically inaccurate due to insufficient sampling. However, in an MMC simulation it is possible for the histogram to be smooth when it is inaccurate due to correlations between the  $P_k^j$  [33]. Such correlations are due to the nature of the update in the biasing pdfs that is performed between iterations. Therefore, despite the stringent stopping conditions described above, it is possible that there could be systematic errors in the MMC simulations that are significantly larger than 10%. To check for such systematic errors in the pdf, we reran two of the MMC simulations five times each with different seeds for the random number generator. In both cases, the five pdfs were indistinguishable when viewed on a log scale. The mean of the maximum relative error between the pdfs for all 20 possible pairs of runs at the final iteration was less than 0.6 in both cases, and the standard deviation was less than 0.5. These five different runs are statistically independent and give us confidence that any systematic errors in our MMC simulations were small and, in particular, are smaller than the difference between the MMC results and the results that we obtained using the other three noise methods.

### C. Code Validation

All four noise methods were reimplemented and validated for this study. First, we obtained excellent agreement between all four methods for a back-to-back system consisting of a transmitter, ASE noise source, and a receiver. Second, we obtained agreement for propagation through a long-haul transmission system in the case of an artificially low-nonlinear index in the fibers. Third, we reproduced the agreement between the NCM and MMC methods for the system used in [21]. In this case, the AWGN method was in excellent agreement with both the NCM and MMC methods. Finally, we performed a separate validation of the NCM method by comparison to an analytical formula that is valid in the case of transmission of a CW signal through a nonlinear fiber with no loss and no dispersion, followed by an integrate-and-dump receiver. Although we obtained excellent agreement between the analytical formula and our numerical implementation of the NCM method, in this case the NCM does

not agree with the results of MMC simulations due to noise inflation about the central frequency that cannot be modeled using linearization as is discussed in [15], [16]. Therefore, we have not included the analytical formula here.

### III. TEST SYSTEMS

We used two long-haul single-channel 10 Gb/s RZ systems in our study. Each system is based on a single channel of a commercial undersea WDM system. System I resembles one of the first commercial undersea WDM systems [34] and has been extensively studied [13], [21], [35]–[37]. System II is a WDM system with slope-matched transmission fibers that resembles the system in [38] and was used in studies of collision-induced timing jitter [39]–[41].

For both systems, we used a chirped raised cosine modulation format with a chirp parameter of  $-0.6$  [42]. We used a 32-bit de Bruijn pseudo-random bit sequence with an optical extinction ratio of 20 dB in the spaces. The central wavelength of the channel and peak power of the pulses was varied to simulate a range of channels and power levels. The receiver consisted of an optical filter, photodetector, and an electric filter. The optical filter was a third-order super-Gaussian filter with a full-width at half-maximum (FWHM) of 35 GHz [41], and the electric filter was a fifth-order Bessel filter with a 3-dB bandwidth of 8 GHz. In all four noise models, we manually set the clock recovery time to be the center of the bit slot so as to avoid statistical uncertainties that occur in the Monte Carlo methods when the clock is recovered automatically.

For both systems, the transmission system consisted of a dispersion compensating fiber (pre-DCF) followed by a number of periods of the dispersion map and finally another dispersion compensating fiber (post-DCF). The dispersion values of the pre- and post-DCF fibers were chosen independently of each other and depended on the central wavelength and peak power of the signal. For simplicity, both the pre- and post-DCF fibers were linear and lossless with zero dispersion slope.

System I consisted of 34 periods of a 180 km dispersion map for a total propagation distance of 6120 km. Within the dispersion map, the transmission fiber was DSF, and dispersion compensation was performed using a single-mode fiber (SMF). The dispersion map fibers consisted of 10 km of SMF followed by 160 km of DSF and finally another 10 km of SMF. Optical amplifiers with a gain of 9 dB and a spontaneous emission factor of 2.0 were positioned every 45 km. The gain of the amplifiers exactly balanced the 0.2 dB/km loss of the fibers. The dispersion was  $-2.125$  ps/(nm-km) for the DSF and 17 ps/(nm-km) for the SMF at 1550 nm. For both types of fiber, the dispersion slope was  $0.075$  ps/(nm<sup>2</sup>-km), the nonlinear index was  $2.6 \times 10^{-20}$  m<sup>2</sup>/W, and the effective area was  $50 \mu\text{m}^2$ .

We studied a low-power and a high-power case of System I. In the low-power case, the peak power of the pulses in the transmitter was 1 mW and in the high-power case it was 4 mW. The OSNR just prior to the receiver was 15 dB–0.2 nm in the low-power case and 20.6 dB–0.2 nm in the high-power case.

Because the average dispersion slope of the map is nonzero, we studied single-channel propagation at various central wavelengths chosen from those of a WDM system with a 100 GHz channel spacing and the central channel at 1550.0 nm. These

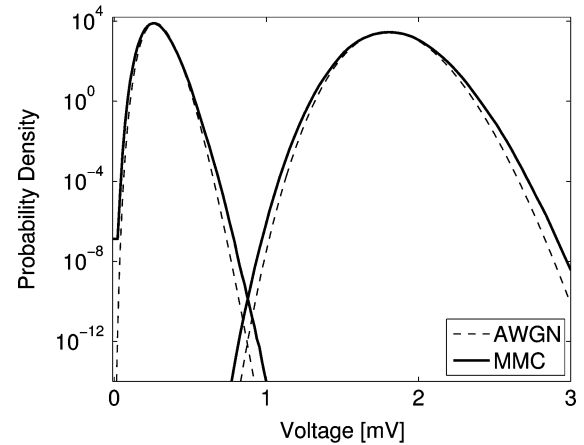


Fig. 1. Probability density functions of the received current in the worst space and worst mark for System II. The results for the AWGN and MMC methods are shown with dashed and solid lines, respectively. The results for the NCM method, with and without phase jitter removal, are indistinguishable from the AWGN results and hence are not included in the figures. Here, and in subsequent figures, probability densities are given in units of probability per mV.

TABLE I

DISPERSION VALUES FOR EACH OF NINE CENTRAL WAVELENGTHS,  $\lambda_{\text{Ch}}$ , FOR SINGLE-CHANNEL PROPAGATION IN SYSTEM I. THESE CENTRAL WAVELENGTHS ARE CHOSEN TO BE THOSE OF NINE CHANNELS IN A WDM SYSTEM WITH A 100 GHz CHANNEL SPACING. COLUMNS 3–6 SHOW THE AVERAGE MAP DISPERSION,  $D_{\text{Map}}$ , AMOUNTS OF PREDISPERSION COMPENSATION,  $D_{\text{Pre}}$ , AND RESIDUAL DISPERSION AT THE RECEIVER IN THE LOW- AND HIGH-POWER CASES,  $D_{\text{Low,Res}}$  AND  $D_{\text{High,Res}}$ , RESPECTIVELY, AT  $\lambda_{\text{Ch}}$  IN PS/NM

Channel Number	$\lambda_{\text{Ch}}$ [nm]	$D_{\text{Map}}$ [ps/nm]	$D_{\text{Pre}}$ [ps/nm]	$D_{\text{Low,Res}}$ [ps/nm]	$D_{\text{High,Res}}$ [ps/nm]
-16	1537.2	-172.8	2940	-85	-585
-8	1543.6	-86.4	1450	-38	-438
-4	1546.8	-43.2	540	1	501
-2	1548.4	-21.6	300	116	-334
0	1550.0	0	100	100	-100
2	1551.6	21.6	-200	34	1234
4	1553.2	43.2	-850	-251	349
8	1556.4	86.4	-1570	-2	-102
16	1562.8	172.8	-2850	-175	-175

channels therefore had different average map dispersions and required differing amounts of pre- and postdispersion compensation. Initially, we chose the amounts of pre- and postdispersion compensation to optimize the eye opening of the noise-free signal. However, because we were only simulating one channel of a WDM system, it was necessary to adjust the amount of postdispersion compensation so that the BER was greater than about  $10^{-13}$ . If the BER was much lower, the MMC simulations became too computationally expensive. In Table I, we show the central wavelengths of each of the nine channels we studied, together with the average map dispersion, the amount of predispersion compensation, and the residual dispersion at the receiver in the low- and high-power cases at each of these wavelengths. In the low-power case, the amount of postdispersion compensation was approximately the same as that of the predispersion compensation except for channels  $-8$ ,  $-4$ , and  $0$ .

System II consisted of 100 periods of a 51.44 km dispersion map for a total propagation distance of 5144 km. The dispersion

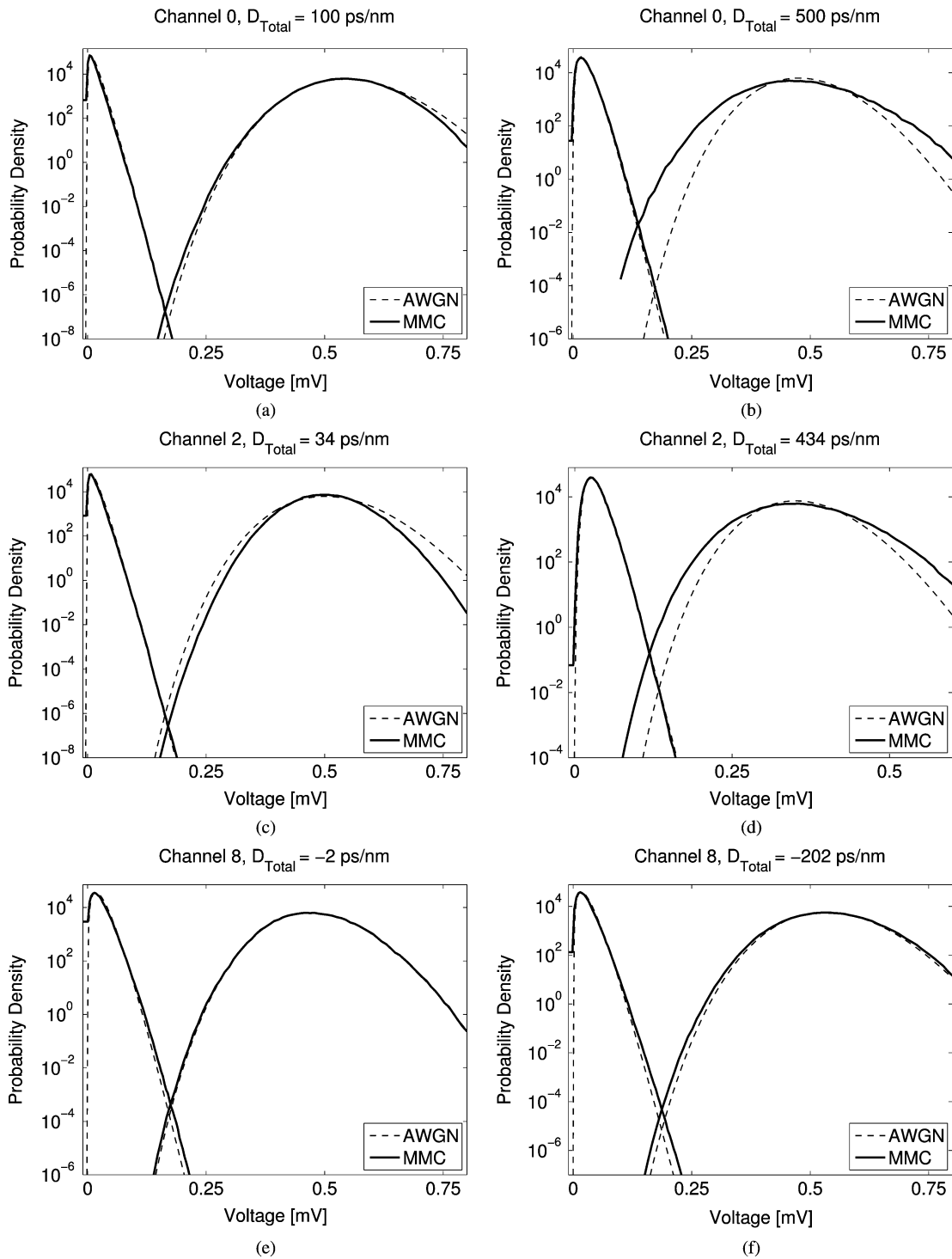


Fig. 2. Probability density functions of the received current in the worst space and worst mark for the low-power case of System I. The results for the small amounts of residual dispersion given in Table I are shown in the left column and those for large amounts of residual dispersion are shown in the right column. (a) Channel 0 with residual dispersion  $D_{Res} = 100$  ps/nm; (b) Channel 0 with  $D_{Res} = 500$  ps/nm; (c) Channel 2 with  $D_{Res} = 34$  ps/nm; (d) Channel 2 with  $D_{Res} = 434$  ps/nm; (e) Channel 8 with  $D_{Res} = -2$  ps/nm; (f) Channel 8 with  $D_{Res} = -202$  ps/nm. The results for the AWGN and MMC methods are shown with dashed and solid lines, respectively. The results for the NCM method, with and without phase jitter removal, are indistinguishable from the AWGN results and hence are not included in the figures.

map and pre- and postdispersion compensation were optimized using a procedure described in [41]. However, for the results in this paper, the amount of post-DCF was about 600 ps/nm larger than in [41] in order to produce a nonoptimal BER with the AWGN method on the order of  $10^{-17}$  with single-channel propagation. Within the dispersion map, the transmission fiber

was  $D_+$  fiber, and dispersion compensation was performed using slope-matched  $D_-$  fiber. The dispersion map fibers consisted of 34 km of  $D_+$  fiber followed by 17.44 km of  $D_-$  fiber and an amplifier. The amplifier had a gain of 10.82 dB and an artificially high spontaneous emission factor of 3.0 was chosen so that for single-channel propagation the BER was greater

TABLE II  
BER FOR THE LOW-POWER CASE OF SYSTEM I WITH THE AMOUNTS OF RESIDUAL DISPERSION AS SHOWN IN TABLE I. IN COLUMNS 2 AND 3, WE TABULATE THE BER FOR EACH CHANNEL OBTAINED USING THE PDFS OF THE RECEIVED CURRENT IN ALL 32 BITS WITH THE AWGN AND NCM METHODS, RESPECTIVELY

Ch.	AWGN	NCM
-16	$4 \times 10^{-12}$	$3 \times 10^{-12}$
-8	$8 \times 10^{-12}$	$6 \times 10^{-12}$
-4	$9 \times 10^{-12}$	$7 \times 10^{-12}$
-2	$3 \times 10^{-11}$	$2 \times 10^{-11}$
0	$4 \times 10^{-13}$	$2 \times 10^{-13}$
2	$2 \times 10^{-12}$	$2 \times 10^{-12}$
4	$5 \times 10^{-12}$	$4 \times 10^{-12}$
8	$1 \times 10^{-10}$	$1 \times 10^{-10}$
16	$2 \times 10^{-8}$	$2 \times 10^{-8}$

than  $10^{-17}$ . The pre-DCF fiber consisted of 51 km of  $D_+$  fiber, and the post-DCF fiber consisted of 120 km of  $D_+$  fiber. The average map dispersion was  $-26$  ps/nm and the residual dispersion at the receiver was 872 ps/nm at 1550 nm. For the  $D_+$  and  $D_-$  fibers, the dispersion was 20.17 ps/(nm-km) and  $-40.8$  ps/(nm-km) at 1550 nm, the dispersion slope was 0.062 ps/(nm<sup>2</sup>-km) and  $-0.124$  ps/(nm<sup>2</sup>-km), the nonlinear index was  $1.7 \times 10^{-20}$  m<sup>2</sup>/W and  $2.2 \times 10^{-20}$  m<sup>2</sup>/W, the effective area was 106.7  $\mu\text{m}^2$  and 31.1  $\mu\text{m}^2$  and the loss was 0.19 dB/km and 0.25 dB/km, respectively. Because the fibers were slope-matched, we only propagated a signal at the central frequency of 1550 nm. The peak power of the pulses was 5 mW. The OSNR just prior to the receiver was 21 dB-0.2 nm.

#### IV. RESULTS

We begin with the results for the low-power case of System I and for System II. For System I, we studied nine single-channel systems propagating at each of the nine central wavelengths in Table I. In Table II, we show the BER values for each channel of System I obtained using the pdfs of the received current in all 32 bits with the AWGN and NCM methods, respectively. For System II, the BER values obtained using all 32 bits were  $2 \times 10^{-17}$  and  $1 \times 10^{-17}$  for the AWGN and NCM methods, respectively. In all cases, the BERs for the AWGN and NCM methods agree to within a factor or two or less. In the NCM method, phase jitter was removed from the covariance matrix at each amplifier. However, we also applied the NCM method without phase jitter removal and found that there was no difference in the results. This result shows that, unlike in highly nonlinear dispersion-managed soliton systems [11], the NCM method does not breakdown in quasi-linear systems due to rapid growth of phase jitter.

In order to compare the MMC method with the AWGN method, we also calculated the BER based on the worst mark and space. In Table III, we show the BER obtained from the pdfs in the worst space and worst mark with the AWGN, NCM, and MMC methods, respectively. The BERs obtained using the AWGN method are within a factor of four or less of the BERs obtained using the MMC method. The corresponding BERs for System II were  $7 \times 10^{-18}$ ,  $6 \times 10^{-18}$ , and  $3 \times 10^{-15}$  for the AWGN, NCM and MMC methods, respectively. In this

TABLE III  
BER FOR THE LOW-POWER CASE OF SYSTEM I WITH THE AMOUNTS OF RESIDUAL DISPERSION AS SHOWN IN TABLE I. IN COLUMNS 2, 3, AND 4, WE TABULATE THE BER FOR EACH CHANNEL OBTAINED USING THE PDFS OF THE RECEIVED CURRENT IN THE WORST SPACE AND WORST MARK WITH THE AWGN, NCM, AND MMC METHODS, RESPECTIVELY

Ch.	AWGN	NCM	MMC
-16	$3 \times 10^{-11}$	$2 \times 10^{-11}$	$1 \times 10^{-11}$
-8	$4 \times 10^{-11}$	$3 \times 10^{-11}$	$1 \times 10^{-10}$
-4	$2 \times 10^{-11}$	$2 \times 10^{-11}$	$1 \times 10^{-11}$
-2	$4 \times 10^{-11}$	$3 \times 10^{-11}$	$1 \times 10^{-11}$
0	$3 \times 10^{-13}$	$1 \times 10^{-13}$	$3 \times 10^{-13}$
2	$3 \times 10^{-12}$	$3 \times 10^{-12}$	$1 \times 10^{-12}$
4	$3 \times 10^{-12}$	$2 \times 10^{-12}$	$8 \times 10^{-12}$
8	$1 \times 10^{-9}$	$8 \times 10^{-10}$	$3 \times 10^{-9}$
16	$2 \times 10^{-7}$	$2 \times 10^{-7}$	$7 \times 10^{-7}$

TABLE IV  
BER FOR SELECTED CHANNELS IN THE LOW-POWER CASE OF SYSTEM I WITH THE LARGE AMOUNTS OF RESIDUAL DISPERSION GIVEN IN COLUMN 2. IN COLUMNS 3 AND 4, WE TABULATE THE BER FOR EACH CHANNEL OBTAINED USING THE PDFS OF THE RECEIVED CURRENT IN THE WORST SPACE AND WORST MARK WITH THE AWGN AND MMC METHODS, RESPECTIVELY. THE RESULTS OBTAINED USING THE NCM, WITH AND WITHOUT PHASE JITTER REMOVAL (NOT SHOWN), ARE VERY SIMILAR TO THOSE OBTAINED USING THE AWGN METHOD

Ch. Num.	$D_{\text{Total}}$ [ps/nm]	AWGN Worst Bits	MMC Worst Bits
-8	-438	$4 \times 10^{-8}$	$3 \times 10^{-7}$
-2	-284	$4 \times 10^{-11}$	$1 \times 10^{-11}$
0	500	$3 \times 10^{-10}$	$8 \times 10^{-8}$
2	434	$8 \times 10^{-8}$	$4 \times 10^{-7}$
8	-202	$4 \times 10^{-11}$	$2 \times 10^{-10}$

case, the AWGN method predicts a BER that is about 500 times smaller than that obtained with the MMC method. To investigate the source of this disagreement, in Fig. 1 we show the pdfs of the received current in the worst space and mark for System II. The results for the AWGN and MMC methods are shown with dashed and solid lines, respectively. We observe that with the MMC method, the tails of both pdfs lie above those obtained with the AWGN method. We do not show the pdfs for the NCM method, with or without phase jitter removal, since they are indistinguishable from the pdfs for the AWGN method.

Results of Hui *et al.* [4] suggest that in systems affected by parametric gain, the system performance can depend significantly on the amount of residual dispersion at the receiver. To investigate the effect that a large residual dispersion has on the level of agreement between the AWGN and MMC methods, we changed the amounts of postdispersion compensation in channels -8, -2, 0, 2, and 8 of System I so as to increase the magnitude of the residual dispersion. The values of residual dispersion we used for these simulations are shown in column two of Table IV and are between 200 and 400 ps/nm different from the original residual dispersion values in Table I. The corresponding BER values obtained from the worst bits using the AWGN and MMC methods are shown in columns three and four of Table IV, respectively. Although the agreement between the two methods

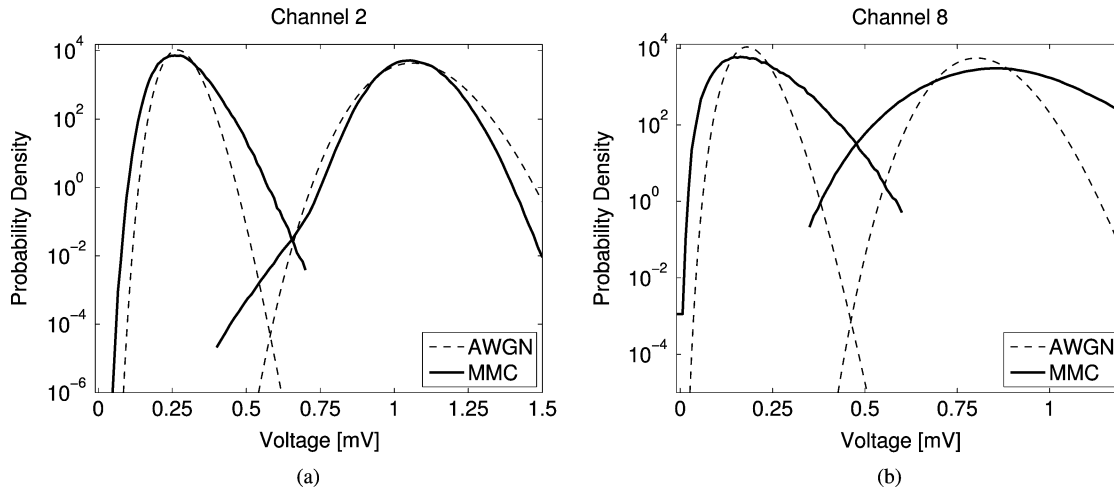


Fig. 3. Probability density functions of the received current in the worst space and worst mark in (a) Channel 2 and (b) Channel 8 for the high-power case of System I. The results for the AWGN and MMC methods are shown with dashed and solid lines, respectively.

is not as good with the larger amounts of residual dispersion, the values are still within a factor of eight of each other except for Channel 0 where the MMC method produces a BER that is 270 times greater than does the AWGN method.

To further investigate the effect of large residual dispersion, in Fig. 2 we show the pdfs of the received current in the worst space and worst mark for Channels 0, 2, and 8 obtained using the AWGN and MMC methods. The line styles are the same as for Fig. 1 and as before we do not show the results for the NCM method as they are indistinguishable from those obtained using the AWGN method. In the left column, we show the results for the smaller amounts of residual dispersion given in Table I, while in the right column we show the results for the larger amounts given in Table IV. The figures show that, with both large and small residual dispersion, the pdf in the worst space is almost the same for the AWGN and MMC methods. However, when the amount of postdispersion compensation is chosen so that the magnitude of the residual dispersion is large, both signal–noise and noise–noise interactions during transmission can have an affect on the pdfs of the marks, which can result in a breakdown of the AWGN method. This effect can be seen in all three cases in Fig. 2. The mean is lower and the standard deviation is higher with the MMC method, and the tails of the MMC pdf lie above those of the AWGN pdf. Moreover, the closer the average map dispersion is to zero, the more pronounced is the disagreement between the two methods. Because of the excellent agreement between the AWGN and NCM methods, we ascribe the breakdown in the AWGN method shown in the right column of Fig. 2 to the inflation of inphase noise due to noise–noise interactions near the central frequency of the signal discussed in [15], [16], which at this low power level only affects the BER when the magnitude of the residual dispersion at the receiver is large relative to the dispersion variation within the dispersion map [4]. Finally, we note that Channel 2 with the lower residual dispersion value and Channel –2 with the higher residual dispersion value exhibit slight noise-squeezing [10], as in these cases nonlinear signal–noise interactions during transmission actually result in a slight decrease of the BER.

To investigate the validity of the AWGN method at high power levels, we now discuss the results for the high-power case of System I. Although the BERs obtained with the AWGN method can be very low for single-channel propagation with the high peak power of 4 mW that we used, there is a large amount of pattern dependence in the received noise-free electrical signal. This pattern dependence is primarily due to the Kerr nonlinearity and to a lesser extent to the nonoptimal amounts of postdispersion compensation we used. For example, the ratio of the largest to the smallest voltage mark is between 1.5 and 3, depending on the channel. Therefore, rather than representing the effects one might encounter in a well-designed commercial point-to-point system, these results are provided to illustrate how badly the AWGN method can breakdown due to some of the more extreme nonlinear signal–noise and noise–noise interactions that could be encountered during system design or possibly after long-distance propagation in an all-optical network.

In Fig. 3, we show the pdfs of the worst space and worst mark for Channels 2 and 8. In both cases, the tails of the MMC pdfs in the spaces lie well above those of the AWGN pdfs, and for Channel 8, the standard deviation in the mark is twice as large for the MMC method as for the AWGN method. Consequently for Channel 8, the BER is  $10^5$  times larger with the MMC method. The pdfs of the marks in Channel 2 exhibit an interesting phenomenon. Although the AWGN and MMC methods agree quite well over five orders of magnitude, at very low probabilities, the MMC pdf suddenly and markedly diverges from that of the AWGN pdf. By rerunning the MMC simulation several times, we checked that the shape of this pdf is not a statistical accident. This phenomenon would be hard to detect using StdMC simulations and was not captured by the NCM method. Based on the similarity to the pdf of the mark in Fig. 4 of [11], we infer that timing jitter is responsible for the knee-like shape of this pdf and is probably due to the very large residual dispersion in this system.

In Table V, we show the  $Q$ -factor for the worst space and mark in the high-power case of System I. In columns two, three, and four, we tabulate the  $Q$ -factor computed from the pdfs of

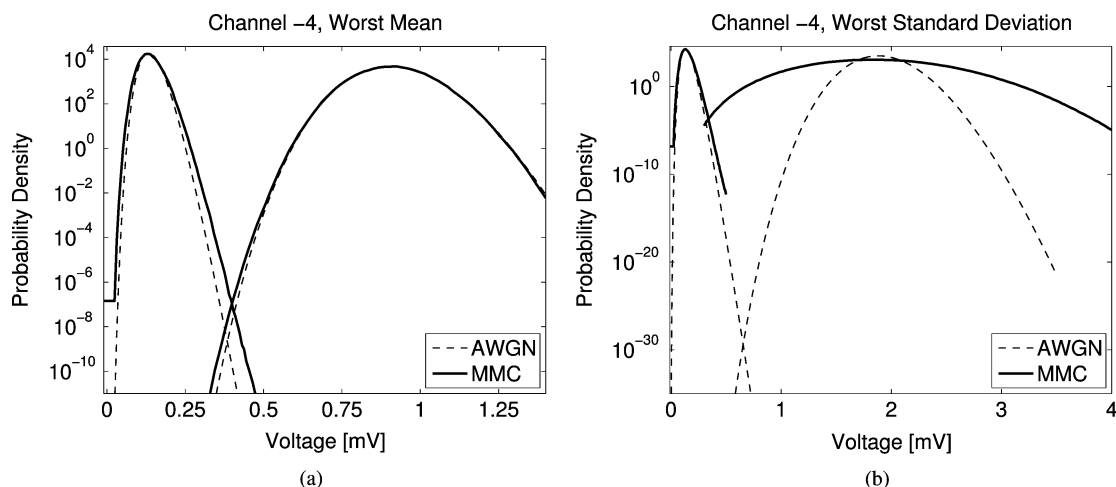


Fig. 4. Probability density functions of the received current in Channel -4 of the high-power case of System I for the space with the worst mean and in (a) the mark with the worst mean and in (b) the mark with the worst standard deviation. Here, the means and standard deviations were calculated using a StdMC simulation. The results for the AWGN and MMC methods are shown with dashed and solid lines, respectively.

TABLE V  
 $Q$ -FACTOR COMPUTED FROM THE WORST SPACE AND WORST MARK IN THE HIGH-POWER CASE OF SYSTEM I, WITH THE AMOUNTS OF RESIDUAL DISPERSION AS SHOWN IN TABLE I. IN COLUMNS 2, 3, AND 4, WE TABULATE THE  $Q$ -FACTORS COMPUTED WITH THE AWGN, NCM, AND MMC METHODS, RESPECTIVELY, THAT WE OBTAINED USING AN ACCURATE RECEIVER MODEL. IN COLUMN 5, WE TABULATE THE  $Q$ -FACTORS COMPUTED USING STDMC SIMULATIONS FROM THE MEAN AND STANDARD DEVIATION IN THE WORST SPACE AND WORST MARK

Ch. Num.	AWGN Acc. Rx.	NCM Acc. Rx.	MMC Acc. Rx.	StdMC Gauss.
-16	6.3	6.4	5.0	5.0
-8	8.5	8.6	7.2	7.7
-4	7.6	7.6	7.1	7.2
-2	7.0	7.1	6.2	5.8
0	6.9	6.9	5.6	5.5
2	6.1	6.3	4.8	5.9
4	6.3	6.5	5.4	5.5
8	5.7	5.7	3.1	3.1
16	6.1	6.2	4.4	4.8

the received current that were obtained using the AWGN, NCM, and MMC methods with an accurate receiver model. The NCM results are slightly different from the AWGN results, but both produce  $Q$ -factors that are significantly larger than those obtained using the MMC method. These results suggest that at this high power level parametric gain involving only signal-noise interactions is beginning to play a slight role, but that, as in the low-power case, the breakdown of the AWGN method is primarily due to quadratic and higher-order nonlinear noise-noise interactions such as those discussed by Serena *et al.* in [15], [16].

In column five of Table V, we show the  $Q$ -factor computed from the mean and standard deviation in the worst space and mark using a StdMC simulation. The agreement between the  $Q$ -factors computed using the standard and MMC simulations is quite good. A similar level of agreement (not shown) was obtained for the low-power case of System I and for System II. Bosco *et al.* [9] claimed that in the presence of parametric gain, the  $Q$ -factor could not be reliably computed using the Gaussian

approximation to the pdfs of the received current. However, their argument was based on simulations of a short 50 km system with a 50-mW high-power CW signal. Due to its atypically large powers, this system produced an asymmetrical pdf for the mark. By contrast, the results we obtained in Table V for a long-haul system with typical powers show very good agreement between the  $Q$ -factors computed using the Gaussian approximation and those obtained using MMC. The only exception is for Channel 2, where the  $Q$ -factor computed using the MMC simulation is somewhat lower than that predicted by the StdMC simulation due to the bent knee in the pdf of the mark.

A major disadvantage of the MMC method is that, particularly in the presence of large pattern dependence in the noise-free signal, a separate MMC simulation must be run to calculate the pdf in each bit. So far, all our MMC results have been for the worst space and mark in the electrically filtered noise-free signal. However, using StdMC simulations we observed that, for some channels in the high-power case of System I, the mark that produced the worst  $Q$ -factor was actually the one with the largest standard deviation, rather than that with the smallest mean. In Fig. 4, we show the pdfs in Channel -4 of the high-power case of System I for (a) the mark with the worst mean and (b) the mark with the worst standard deviation. In both (a) and (b) we used the space with the worst mean. The corresponding BERs are  $5 \times 10^{-13}$  and  $4 \times 10^{-9}$  for the marks with the worst mean and worst standard deviation, respectively. The mechanism responsible for this result is as follows: The noise in the mark with the worst standard deviation undergoes greater parametric gain during transmission because this mark is the central mark in a string of five marks and hence the signal power is always much higher than for the mark with the worst mean, which is an isolated mark. The noise with large parametric gain then beats with a large power signal in the receiver to produce a very large standard deviation in the mark with the worst standard deviation. Consequently, MMC simulations may not be an effective way to calculate the BER for higher power systems unless all bits in the simulation are kept which is prohibitively time consuming at the time of this writing.

TABLE VI

THE  $Q$ -FACTOR COMPUTED USING ALL 32 BITS IN BOTH THE LOW AND HIGH POWER CASES OF SYSTEM I, WITH THE AMOUNTS OF RESIDUAL DISPERSION AS SHOWN IN TABLE I. RESULTS FROM THE LOW POWER CASE ARE SHOWN IN COLUMNS 2 (AWGN) AND 3 (StdMC) AND THOSE FOR THE HIGH POWER CASE IN COLUMNS 4 (AWGN) AND 5 (StdMC). FOR THE AWGN METHOD WE TABULATE THE  $Q$ -FACTOR OBTAINED USING THE ACCURATE RECEIVER MODEL AND FOR THE STANDARD MONTE CARLO METHOD WE TABULATE THE  $Q$ -FACTOR OBTAINED FROM THE GAUSSIAN PDFS IN EACH BIT

Ch. Num.	AWGN Acc. Rx. Low	StdMC Gauss. Low	AWGN Acc. Rx. High	StdMC Gauss. High
-16	6.8	6.8	6.0	4.9
-8	6.7	6.7	6.9	5.8
-4	6.7	6.9	6.9	4.5
-2	6.6	6.5	7.3	5.9
0	7.2	7.3	6.9	5.8
2	6.9	7.4	6.3	4.1
4	6.8	6.2	6.3	5.6
8	6.3	6.1	6.0	3.9
16	5.5	5.4	5.5	4.2

Taken together, these results suggest that the quickest and easiest way to reliably ascertain the accuracy of the AWGN method is to perform a StdMC simulation with a computational time of several hundred times that of a single noise-free simulation. In Table VI, we perform a final test of the validity of the AWGN method by comparing the  $Q$ -factors computed using the AWGN method with an accurate receiver model to the  $Q$ -factors obtained from the Gaussian pdfs that we compute using StdMC simulations in both the low- and high-power cases of System I. These results were obtained using all 32 bits. Recall that when white Gaussian noise is added to a RZ signal without pattern dependence, the  $Q$ -factor computed from the Gaussian pdfs is slightly smaller than the accurate  $Q$ -factor, provided the accurate  $Q$ -factor is more than 3. The agreement between the two methods is very good when the peak power of the pulses in the transmitter is 1 mW (the low-power case). However, the AWGN method breaks down when the peak power is 4 mW (the high-power case). The corresponding results for System II are a  $Q$ -factor of 8.4 ( $\text{BER} = 2 \times 10^{-17}$ ) with the AWGN method and a  $Q$ -factor of 7.9 ( $\text{BER} = 1 \times 10^{-15}$ ) with a StdMC simulation. Although the peak power at the transmitter in System II was 5 mW, nonlinear signal–noise and noise–noise interactions during fiber propagation do not affect the  $Q$ -factor as much as in the high-power case of System I since the nonlinearity of the  $D_+$  transmission fiber in System II is only 30% of that in System I.

## V. CONCLUSION

On the basis of the simulations discussed earlier, we conclude that for long-haul, quasi-linear, RZ, direct-detection transmission systems with typical peak power levels of about 1 mW in which the residual dispersion at the receiver is within 200 ps/nm of zero, nonlinear interactions involving the signal and noise during transmission have a negligible effect on the system performance. For such systems, the AWGN method provides a

reliable approximation to the BER. However, when the post-dispersion compensation is chosen so that the absolute residual dispersion exceeds 200 ps/nm, the AWGN and NCM methods may simultaneously breakdown, particularly when the average map dispersion is close to zero. Although they were obtained for a single-channel system, it is reasonable to assume that these results will also hold for WDM systems since in [14] we obtained excellent agreement between the NCM method and MMC simulations for a dense WDM system similar to the low-power case of System I. However, intrachannel signal–noise interactions compete in these systems with quasi-random interchannel signal–signal interactions, which make the signal–noise interactions difficult to observe in typical systems. When the peak power level is increased to about 4 mW, the AWGN method breaks down.

Although the specific power levels and dispersion values at which the AWGN method breaks down in a quasi-linear system will vary somewhat from system to system, our results strongly indicate that when the AWGN method fails, the power level will already be so large that the system performance will be significantly impaired due to pattern dependences in the noise-free signal. We also observe that despite its success in modeling highly nonlinear dispersion-managed soliton systems, we have not found any quasi-linear system for which it is advantageous to use the NCM method. In fact, whenever the AWGN and MMC methods disagree, the NCM method gives the wrong result.

At present, there is no computationally rapid deterministic method that is capable of accurately modeling inphase noise inflation near the central frequency of the channel due to parametric gain that is pumped by data-modulated noise-free signals. It may be possible that the methods that Serena *et al.* [15], [16] and Secondini *et al.* [17] developed for CW signals can be generalized to accurately treat data-modulated signals. In the meantime, we suggest that to detect breakdown in the AWGN method at high power levels one should estimate the  $Q$ -factor from the mean and standard deviation of the received current in each bit using a limited number of StdMC simulations. One should then compare this mean and standard deviation to the mean and standard deviation that are calculated using the AWGN method. When they disagree, the AWGN method is no longer reliable.

## ACKNOWLEDGMENT

The authors thank Peter Winzer for sharing his insights on the AWGN model. They also thank Ronald Holzlohner, Walter Pellegrini, Marco Secondini, Oleg Sinkin, Anshul Kalra, and Aurenice Oliveira for helpful discussions. One of the authors (J.Z.) thanks UMBC for support while on leave during Spring 2007 and is grateful to the Mathematics Department at The University of Texas at Austin for its hospitality.

## REFERENCES

- [1] G. P. Agrawal, *Fiber-Optic Communication Systems*, 2nd ed. New York: John Wiley and Sons, Inc., 1997.

- [2] G. P. Agrawal, *Nonlinear Fiber Optics*, 2nd ed. London: Academic Press, 1995.
- [3] R. Hui, D. Chowdhury, M. Newhouse, M. O'Sullivan, and M. Poettercker, "Nonlinear amplification of noise in fibers with dispersion and its impact in optically amplified systems," *IEEE Photon. Technol. Lett.*, vol. 9, no. 3, pp. 392–394, Mar. 1997.
- [4] R. Hui, M. O'Sullivan, A. Robinson, and M. Taylor, "Modulation instability and its impact in multispan optical amplified IMDD systems: Theory and experiments," *J. Lightw. Technol.*, vol. 15, pp. 1071–1081, Jul. 1997.
- [5] A. N. Pilipetskii, V. J. Mazurczyk, and C. J. Chen, "The effect of dispersion compensation on system performance when nonlinearities are important," *IEEE Photon. Technol. Lett.*, vol. 11, no. 2, pp. 284–286, Feb. 1999.
- [6] E. A. Golovchenko, A. N. Pilipetskii, N. S. Bergano, C. R. Davidson, F. I. Khatri, R. M. Kimball, and V. J. Mazurczyk, "Modeling of transoceanic fiber-optic WDM communications systems," *IEEE J. Sel. Topics Quantum Electron.*, vol. 6, no. 2, pp. 337–347, Mar./Apr. 2000.
- [7] A. Carena, V. Curri, R. Gaudino, P. Poggiolini, and S. Benedetto, "New analytical results on fiber parametric gain and its effects on ASE noise," *IEEE Photon. Technol. Lett.*, vol. 9, no. 4, pp. 535–537, Apr. 1997.
- [8] G. Bosco, A. Carena, V. Curri, R. Gaudino, P. Poggiolini, and S. Benedetto, "A novel analytical method for the BER evaluation in optical systems affected by parametric gain," *IEEE Photon. Technol. Lett.*, vol. 12, no. 2, pp. 152–154, Feb. 2000.
- [9] G. Bosco, A. Carena, V. Curri, R. Gaudino, P. Poggiolini, and S. Benedetto, "A novel analytical approach to the evaluation of the impact of fiber parametric gain on the bit error rate," *IEEE Trans. Commun.*, vol. 49, no. 12, pp. 2154–2163, Dec. 2001.
- [10] R. Hui and M. O'Sullivan, "Noise squeezing due to Kerr effect nonlinearities in optical fibers with negative dispersion," *Electron. Lett.*, vol. 32, no. 21, pp. 2001–2003, 1996.
- [11] R. Holzlöhner, C. R. Menyuk, V. S. Grigoryan, and W. L. Kath, "Accurate calculation of eye diagrams and error rates in long-haul transmission systems using linearization," *J. Lightw. Technol.*, vol. 20, pp. 389–400, 2002.
- [12] R. Holzlöhner, C. R. Menyuk, W. L. Kath, and V. S. Grigoryan, "A covariance matrix method to compute accurate bit error rates in a highly nonlinear dispersion-managed soliton system," *IEEE Photon. Technol. Lett.*, vol. 15, no. 5, pp. 688–690, May 2003.
- [13] R. Holzlöhner, C. R. Menyuk, W. L. Kath, and V. S. Grigoryan, "Efficient and accurate computation of eye diagrams and bit-error rates in a single-channel CRZ system," *IEEE Photon. Technol. Lett.*, vol. 14, no. 8, pp. 1079–1081, Aug. 2002.
- [14] W. Pellegrini, J. Zweck, C. R. Menyuk, and R. Holzlöhner, "Computation of bit error ratios for a dense WDM system using the noise covariance matrix and multicanonical Monte Carlo methods," *IEEE Photon. Technol. Lett.*, vol. 17, no. 8, pp. 1644–1646, Aug. 2005.
- [15] P. Serena and A. Bononi, "Power threshold due to parametric gain in dispersion-mapped communication systems," *IEEE Photon. Technol. Lett.*, vol. 14, no. 11, pp. 1521–1523, Nov. 2002.
- [16] P. Serena, A. Bononi, J.-C. Antona, and S. Bigo, "Parametric gain in the strongly nonlinear regime and its impact on 10 Gb/s NRZ systems with forward-error correction," *J. Lightw. Technol.*, vol. 23, no. 8, pp. 2352–2363, 2005.
- [17] M. Secondini, E. Forestieri, and C. R. Menyuk, "A novel perturbation method for signal-noise interaction in nonlinear dispersive fibers," in *Proc. OFC'2006*, Anaheim, CA, paper OThD3.
- [18] B. A. Berg and T. Neuhäus, "Multicanonical algorithms for first order phase transitions," *Phys. Lett. B*, vol. 267, pp. 249–253, 1991.
- [19] D. Yevick, "Multicanonical communication system modeling—Application to PMD statistics," *IEEE Photon. Technol. Lett.*, vol. 14, no. 11, pp. 1512–1514, Nov. 2002.
- [20] D. Yevick, "The accuracy of multicanonical system models," *IEEE Photon. Technol. Lett.*, vol. 15, no. 2, pp. 224–226, Feb. 2003.
- [21] R. Holzlöhner and C. R. Menyuk, "Use of multicanonical Monte Carlo simulations to obtain accurate bit error rates in optical communications systems," *Opt. Lett.*, vol. 28, no. 20, pp. 1894–1896, 2003.
- [22] J.-S. Lee and C.-S. Shim, "Bit-error-rate analysis of optically preamplified receivers using an eigenfunction expansion method in optical frequency domain," *J. Lightw. Technol.*, vol. 12, pp. 1224–1229, 1994.
- [23] E. Forestieri, "Evaluating the error probability in lightwave systems with chromatic dispersion, arbitrary pulse shape and pre- and post-detection filtering," *J. Lightw. Technol.*, vol. 18, pp. 1493–1503, 2000.
- [24] O. Sinkin, R. Holzlöhner, J. Zweck, and C. Menyuk, "Optimization of the split-step Fourier method in modeling optical fiber communications systems," *J. Lightw. Technol.*, vol. 21, no. 1, pp. 61–68, 2003.
- [25] C. R. Menyuk, "Application of multiple-length-scale methods to the study of optical fiber transmission," *J. Eng. Math.*, vol. 36, pp. 113–136, 1999.
- [26] O. Sinkin, V. S. Grigoryan, and C. Menyuk, "Accurate probabilistic treatment of bit-pattern-dependent nonlinear distortions in BER calculations for WDM RZ systems," *J. Lightw. Technol.*, vol. 25, no. 10, pp. 2959–2968, 2007.
- [27] I. Roudas, N. Antoniadis, D. H. Richards, R. E. Wagner, J. L. Jackel, S. F. Habiby, T. E. Stren, and A. Elrefaie, "Wavelength domain simulation of multiwavelength optical networks," *J. Sel. Topics Quantum Electron.*, vol. 6, no. 2, pp. 348–362, 2000.
- [28] D. Wang and C. R. Menyuk, "Calculation of penalties due to polarization effects in a long-haul WDM system using a Stokes parameter model," *J. Lightw. Technol.*, vol. 19, pp. 487–494, 2001.
- [29] N. L. Johnson and S. Kotz, *Continuous Univariate Distributions—2*. Boston, MA: Houghton Mifflin, 1970.
- [30] D. Marcuse, "Derivation of analytical expressions for the bit-error probability in lightwave systems with optical amplifiers," *J. Lightw. Technol.*, vol. 8, no. 12, pp. 1816–1823, 1990.
- [31] S. Jaschke, C. Klüppelberg, and A. Lindner, "Asymptotic behavior of tails and quantiles of quadratic forms of Gaussian vectors," *J. Multivariate Anal.*, vol. 88, no. 2, pp. 252–273, 2004.
- [32] M. Pfennigbauer, M. M. Strasser, M. Pauer, and P. J. Winzer, "Dependence of optically preamplified receiver sensitivity on optical and electrical filter bandwidths—Measurement and simulation," *IEEE Photon. Technol. Lett.*, vol. 14, no. 6, pp. 831–833, Jun. 2002.
- [33] A. O. Lima, I. T. Lima Jr., and C. R. Menyuk, "Error estimation in multicanonical Monte Carlo simulations with applications to polarization-mode-dispersion emulators," *J. Lightw. Technol.*, vol. 23, pp. 3781–3789, 2005.
- [34] N. S. Bergano, C. R. Davidson, C. J. Chen, B. Pedersen, M. A. Mills, N. Ramanujam, H. D. Kidorf, A. B. Puc, M. D. Levonas, and H. Abdelkader, "640 Gb/s transmission of sixty-four 10 Gb/s WDM channels over 7200 km with 0.33 (bits/s)/Hz spectral efficiency," in *Tech. Dig. Conf. Opt. Fiber Commun.*, San Diego, CA, 1999, paper PD2.
- [35] R.-M. Mu, T. Yu, V. S. Grigoryan, and C. R. Menyuk, "Dynamics of the chirped return-to-zero modulation format," *J. Lightw. Technol.*, vol. 20, no. 1, pp. 47–57, 2002.
- [36] R.-M. Mu and C. R. Menyuk, "Convergence of the chirped return-to-zero and dispersion managed soliton modulation formats in WDM systems," *J. Lightw. Technol.*, vol. 20, no. 4, pp. 608–617, Apr. 2002.
- [37] R.-M. Mu and C. R. Menyuk, "Symmetric slope compensation in a long-haul WDM system using the CRZ format," *IEEE Photon. Technol. Lett.*, vol. 13, no. 8, pp. 797–799, Aug. 2001.
- [38] J.-X. Cai, M. Nissov, A. N. Pilipetskii, C. R. Davidson, R. M. Mu, M. A. Mills, L. Xu, D. Foursa, R. Menges, P. C. Corbett, D. Sutton, and N. S. Bergano, "1.28 Tb/s (32 × 40 Gb/s) transmission over 4500 km," in *Proc. ECOC'2001*, Amsterdam, Holland, postdeadline paper PDM12.
- [39] O. V. Sinkin, V. S. Grigoryan, J. Zweck, C. R. Menyuk, A. Docherty, and M. Ablowitz, "Calculation, characterization, and application of the time shift function in wavelength-division-multiplexed return-to-zero systems," *Opt. Lett.*, vol. 30, pp. 2056–2058, 2005.
- [40] C. D. Ahrens, M. J. Ablowitz, A. Docherty, O. V. Sinkin, V. Grigoryan, and C. R. Menyuk, "Asymptotic analysis of collision-induced timing shifts in return-to-zero quasi-linear systems with predispersion and postdispersion compensation," *Opt. Lett.*, vol. 31, no. 1, pp. 5–7, 2006.
- [41] O. V. Sinkin, "Calculation of bit error rates in optical fiber communications systems in the presence of nonlinear distortion and noise," Ph.D. dissertation, Univ. Maryland, Baltimore County, 2006.
- [42] T.-S. Yang, W. L. Kath, and S. G. Evangelides, "Optimal prechirping for dispersion managed transmission of return-to-zero pulses," in *Tech. Dig. Conf. Opt. Fiber Commun.*, Washington, D.C., 1999, paper ThQ4.



**John Zweck** received the B.Sc. degree (with honors) from the University of Adelaide, South Australia, in 1988, and the Ph.D. degree in mathematics from Rice University, Houston, TX, in 1993.

From 2003 to 2006, he was an Assistant Professor in the Department of Mathematics and Statistics, University of Maryland Baltimore County (UMBC), and from 2000 to 2003 he was a Research Associate in the Department of Computer Science and Electrical Engineering at UMBC. Since 2006, he has been an Associate Professor of mathematics

and statistics and an Affiliate Associate Professor of computer science and electrical engineering at UMBC, Baltimore, MD. He has performed research in differential geometry, human and computer vision, computational anatomy, and modeling of optical systems. His current research interests include modeling of optical fiber communications systems, short-pulse lasers, and photoacoustic spectroscopy sensors. He is the lead developer of software PhoSSiL, the Photonics Systems Simulator Library.

Dr. Zweck is a member of the Society for Industrial and Applied Mathematics.



**Curtis R. Menyuk** (SM'88–F'98) was born on March 26, 1954. He received the B.S. and M.S. degrees from MIT, Cambridge, MA, in 1976, and the Ph.D. degree from UCLA, Los Angeles, CA, in 1981.

He has worked as a Research Associate at the University of Maryland, College Park, and at Science Applications International Corporation, McLean, VA. In 1986, he became an Associate Professor in the Department of Electrical Engineering at the University of Maryland Baltimore County, and he

was the founding member of this department. In 1993, he was promoted to Professor. He was on partial leave from UMBC from Fall, 1996 until Fall, 2002. From 1996 to 2001, he worked part-time for the Department of Defense, codirecting the Optical Networking program at the DoD Laboratory for Telecommunications Sciences, Adelphi, MD. In 2001–2002, he was the Chief Scientist at PhotonEx Corporation. For the last 18 years, his primary research area has been theoretical and computational studies of lasers, nonlinear optics, and fiber-optic communications. He has authored or coauthored more than 200 archival journal publications as well as numerous other publications and presentations. He has also edited three books. The equations and algorithms that he and his research group at UMBC have developed to model optical fiber systems are used extensively in the telecommunications and photonics industry.

Dr. Menyuk is a member of the Society for Industrial and Applied Mathematics and the American Physical Society. He is a fellow of the Optical Society of America and the IEEE. He is a former UMBC Presidential Research Professor.